Spin tranfer dynamics in nano-oscillators: from radio-frequency signal detection to energy recovery and transmission

Mafalda Jotta Garcia
mafalda.jotta@tecnico.ulisboa.pt

Instituto Superior Técnico, Lisboa, Portugal

March 2019

Abstract

We consider vortex-based spin-torque oscillators (STOs). These devices have an rf detection functionality based on two rectification effects: the spin-torque diode and the vortex core expulsion. This functionality can be leveraged for rf energy harvesting, with rf-to-dc conversion efficiency shown to outperform typical semiconductor harvesters, smaller dimensions and lower costs. A major challenge to improve the sensitivity of these systems is to design networks of connected STOs. This thesis is the first approach to this challenge. We study the spin-torque diode response for one STO and compare the results with a system of two similar STOs connected in series. For the two STO case, we measured a sensitivity of half than expected, although the measurements show that the rectification response is the sum of the response from each STO. Vector network analyzer measurements show that between the single and two STO cases there is a decrease of 30% of the injected rf power transmitted due to poor impedance matching of the circuit. This study shows that by tackling the impedance matching of STO arrays, their sensitivity can be scaled with the number of connected STOs for future technological applications.

Keywords: magnetic vortex, spintronics, spin-transfer, energy harvesting, radiofrequency detector.

1. Introduction

Harnessing rf signals is as a promising way to develop self-powered and wireless devices, like sensors, health monitors, or any type of portable electronics. At this moment, devices such as these are constrained by their batteries, which can't be miniaturized and have limited power. Spintronic devices, namely STOs, emerge with significant potential as rf-based devices, due to their nanometric scale and energy efficiency [1].

The field of spintronics started with the discovery of the giant magnetoresistance (GMR) effect (1988). Since then, this discovery has allowed for the improvement of read-heads and storage capabilities in hard-disks. Later on, in 1995, the discovery of tunneling magnetoresistance (TMR) led to the development of non-volatile MRAM memories, which have become interesting candidates to replace semiconductor based memories, such as S-RAM or D-RAM. Spintronic devices were manipulated solely through magnetic fields, until the discovery of the spin-transfer torque (STT) effect, that allows the manipulation of a ferromagnetic material's magnetization through the application of a spin-polarized current. This has pushed the development of novel STT-based devices, such as improved MRAM type memories and STOs, which are the devices studied in this work. Through the application of a spin-polarized current into STOs, their magnetization oscillates due to a compensation of the system's damping and, because of the TMR effect, this oscillation translates into an alternated current.

The goal of this thesis is to study experimentally the potential use of the spin-torque diode effect in vortex-based STOs for energy harvesting applications. Firstly, we characterize the STO's rectification response, its tunability, and sensitivity dependence on external stimuli. We then analyze a first attempt in scaling the detection sensitivity by connecting two STOs with similar properties, comparing the rectification responses in the case where they are connected in series and connected on their own.

2. Background

2.1. Spin-Torque Oscillators

Magnetoresistance (MR) is the effect by which a magnetic material changes its resistance upon application of a magnetic field. MR devices can be seen simply as having a trilayer structure, with two ferromagnetic (FM) layers, and a non-magnetic spacer in between. One of the FM layers has a fixed mag-

netization, while the other has a free magnetization. The resistance of the device varies with the relative direction of both FM layers' magnetization, being maximal in the anti-parallel (AP) configuration and minimum in the parallel (P) configuration. The MR ratio is given by the following expression:

$$MR(\%) = \frac{R_{AP} - R_P}{R_P} \times 100 \quad (1)$$

Due to conservation of angular momentum, the electrons exert a torque, the STT, in the localized electrons' magnetization, causing it to change direction, Fig.1.

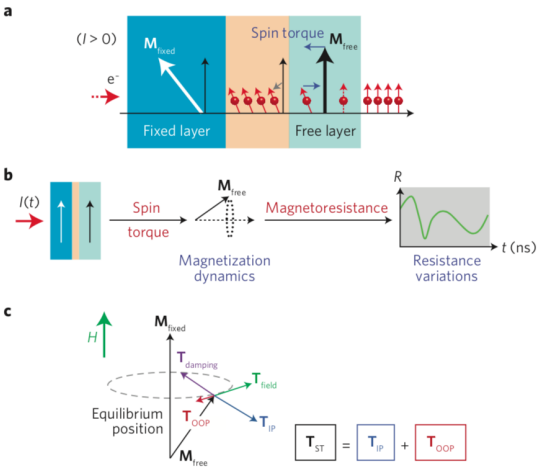

Figure 1: a)Schematic of the STT effect in the layers' magnetizations. b) Operational principal of a magnetoresistive STT device. c) Torques acting on the magnetization upon current injection. Adapted from [2].

2.2. Magnetization dynamics in vortex-based STOs

During this work, we studied STOs with a ferromagnetic free layer which exhibits a vortex magnetization distribution in its equilibrium state, these devices are called vortex-based STOs. The magnetic vortex is composed of two parts, the vortex' body, where the magnetization is aligned with the layer's plane and the vortex core, which has a radius, b, where the magnetization is perpendicular to the layer's plane. The vortex is characterized by two parameters, its polarity (P), which is the direction of the vortex' core magnetization, and its chirality (C), which is the sense of the coiling of the magnetization in the vortex' body.

The Thiele equation describes the dynamics of the vortex' gyrotropic mode by considering the dynamics of a specific point of the magnetization, the vortex core center with position $\mathbf{X_c} = (\rho_c, \chi_c)$. The Thiele equation of motion for the vortex core is given by the following expression:

$$\mathbf{G} \times \frac{d\mathbf{X_c}}{dt} - \mathbf{D}(\mathbf{X_c})\frac{d\mathbf{X_c}}{dt} - \frac{dW}{d\mathbf{X_c}} + \mathbf{F_{stt}} = \mathbf{0} \quad (2)$$

The vortex core dynamics rest on the balance of these four force terms, which are represented in Fig. 2. The first term in Eq. (2.2) is the gyroforce, which is responsible for the rotation of the vortex core around the disk's center. The second term is the damping, which counters the vortex core rotation, while the third term is the confinement, which tends to return the vortex core to the center of the disk, to minimize the total energy of the system. The last term of the Thiele equation corresponds to the STT, $\mathbf{F_{STT}}$, which can be decomposed into the Slonczewski, $\mathbf{F_{Slon}} = \mathbf{F^{\parallel}_{Slon}} + \mathbf{F^{\perp}_{Slon}}$, and field-like torque, $\mathbf{F_{FLT}}$. $\mathbf{F^{\perp}_{Slon}}$ acts as an anti-damping or extra-damping term, depending on the current's direction. For a dc current being injected into the device, the in-plane STT terms $\mathbf{F_{FLT}}$ and $\mathbf{F^{\parallel}_{Slon}}$ act as an in-plane magnetic field, shifting the equilibrium center of the vortex, and can be neglected since they don't excite the vortex gyrotropic mode. It is $\mathbf{F^{\perp}_{Slon}}$ that is responsible for exciting the gyrotropic mode of the vortex in this case [3]. If an ac current, I_rf, is injected into the STO, the in-plane STT terms can no longer be neglected [4].

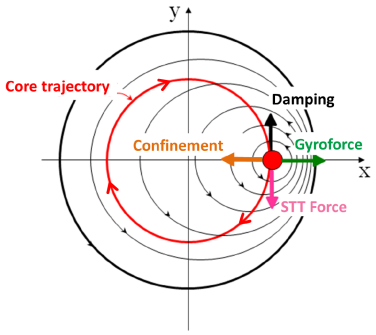

Figure 2: Representation of the forces acting on the vortex core. Adapted from [5].

2.3. Radio-frequency Signal Detection

STOs have a voltage rectification property, which can be leveraged for rf detection and energy harvesting applications. The spin-torque diode effect was first demonstrated in 2005[6]. This effect arises when applying a radio-frequency current, $I = I_{rf}\ \sin(2\pi ft)$, near the free layer's resonance frequency, generating a dc voltage output. It is due to the mixing between the resistance, dependent on the input signal frequency, and the rf current, $V_{dc} = R(f_{res}) \times I_{rf}$. The resonance frequency can be tuned by an external magnetic field, and the output voltage of the spin-torque diode effect is

Table 1: State-of-the-art measured rf detection sensitivities using the spin-torque diode and vortex core expulsion effects.

	Reference	ϵ without dc bias (VW^{-1})	ϵ with dc bias (VW^{-1})
Spin- Torque Diode Effect	Tulapurkar *et al.* [6]	1.4	-
	Miwa *et al.* [7]	630	12,000
	Zhang *et al.* [8]	-	210,000
Vortex Core Expulsion	Jenkins *et al.* [9]	-	40,000
	Tsunegi *et al.* [10]	-	80,000

strongly dependent on I_{rf}, decreasing linearly with the square of the current [6].

The first demonstration of the spin-torque diode effect measured a sensitivity much lower than that of typical semiconductor Schottky diode detectors, 3,800 V W^{-1}, but since then, much higher sensitivities have been reported. Recently, an ultrahigh detection sensitivity of 210,000 V W^{-1} was measured, in the absence of a magnetic field, by taking advantage of injection locking to the external rf source [8].

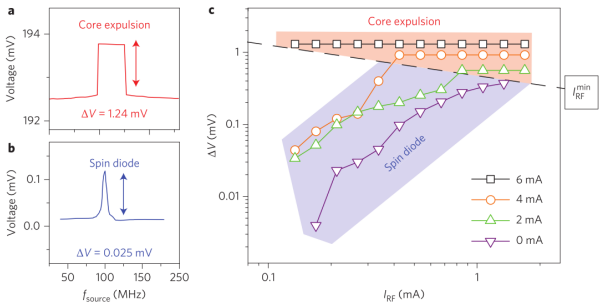

Figure 3: a) Rectification response for the vortex core expulsion ($I_{dc} = 6$ mA) and b) spin-torque diode effect ($I_{dc} = 0$ mA) for $I_{rf} = 0.2$ mA. c) Evolution of the voltage amplitude ΔV in function of the injected I_{rf} for different bias currents I_{dc} at $H_{perp} = 1.5$ kOe. Adapted from [9].

In vortex-based STOs, there is another rectification effect to be considered: vortex core expulsion. When the vortex state is excited by an rf current near the gyrotropic mode of the vortex, the vortex core oscillates with a certain radius, ρ_{osc} [9]. In this configuration the spin-diode effect is observed (Fig.3 (a)). For a large enough rf current, I_{rf}^{min}, the oscillation radius of the magnetization increases, eventually becoming larger than the MTJ radius, and the vortex core is expelled, causing an abrupt variation in the resistance of the device. The rf detection sensitivities, $\epsilon = V_{dc}/P_{rf}$, measured in past works on the subject, are presented in Table 1.

3. Methods

3.1. Samples

The samples used during this project were deposited and patterned at INL - International Iberian Nanotechnology Laboratory, due to an ongoing collaboration between INL, Braga, and UMPhy CNRS/Thales. The samples in the studied chip are circular magnetic tunnel junctions (MTJ) patterned with diameters between 100 nm and 400 nm, in which the free layer presents a vortex configuration in its ground state. The MTJ stack is composed of [Buffer Layer/Synthetic antiferromagnet (SAF)/MgO (1)/$CoFe_{40}B_{20}$ (2)/Ta (0.2)/$NiFe_{30}$ (7)/Cap Layer]. The pinned SAF layer is a [IrMn (6)/$CoFe_{30}$ (2)/Ru (0.7)/$CoFe_{40}B_{20}$ (2)] multilayer. The free layer with a magnetic vortex as the ground state is the permalloy layer. The buffer layer is a [2x[Ta (5)/CuN (50)]/Ta (5)/Ru (5)] multilayer, while the cap layer is Ta (10)/Ru (7). The dimensions inside the parenthesis are in nm.

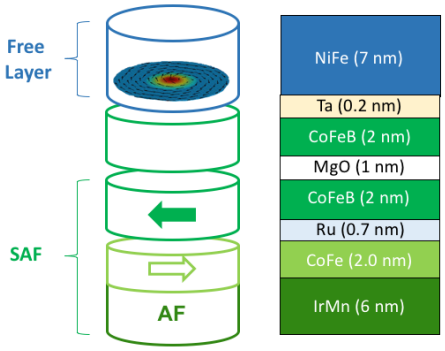

Figure 4: Schematics of the vortex based STO samples studied during this work, with an MgO barrier in between a 7 nm permalloy free layer and a synthetic antiferromagnet polarizer[IrMn (6 nm)/$CoFe_{30}$ (2 nm)/Ru (0.7 nm)/$CoFe_{40}B_{20}$ (2 nm)].

We measured samples with 370 nm, with TMR≈ 40% and an average resistance $R_0 \approx 30\ \Omega$. In this design, each STO has an Al rf line over it, with 300 nm of thickness and 3 μm of width, ∼700 nm away from the free layer. By applying a current through this line a magnetic field parallel to the film's plane is generated.

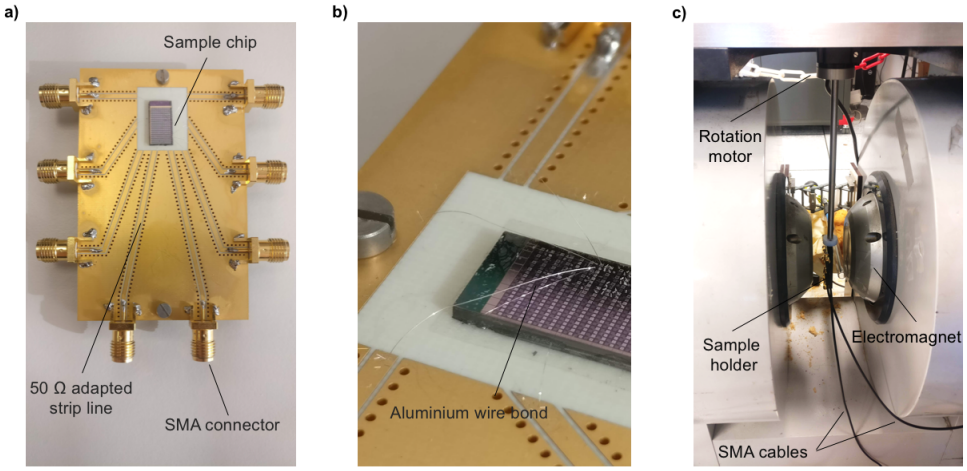

Figure 5: a) Sample holder with 8 SMA pin-outs, the sample is connected through wire bonds between the MTJ electrode pads and 50 Ω adapted lines. b) Wire bonds connecting the sample. c) Sample holder placed in the electromagnet, ready for measurement, connected to the instruments through SMA cables.

3.2. Experimental Procedures

By convention, we chose a positive current corresponding to an electron flux going in the direction from the free layer to the polarizing layer (SAF). The chip is placed on a gold plated sample holder, with 8 SMA pin-outs (Fig. 5(a)). A wire-bonding machine is used to connect the electrodes using aluminum wires (Fig. 5(b)). The bottom electrode of the MTJ is connected to a 50 Ω adapted line, while the top electrode is connected to the sample holder - itself connected to the circuit ground. The sample holder is then placed in a support between the electromagnet coils (Fig. 5(c)). The electromagnet allows us to apply a magnetic field to the sample, between -8 kOe and 8 kOe. It's possible to regulate the angle between the sample and the magnetic field,θ_H, lines through a motor connected to the support. The measurement circuit is schematized in Fig. 6.

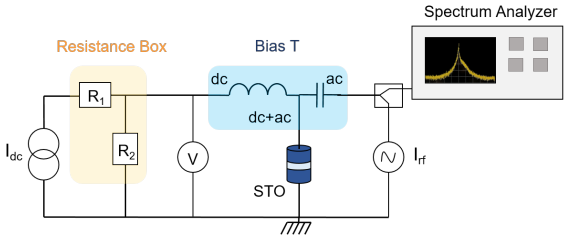

Figure 6: Schematic of the electrical circuit used in the setup during this project.

Both the spectrum analyzer and the signal generator have an impedance $Z_0 = 50\ \Omega$, as do the SMA cables and the connector lines in the sample holder. The different components are connected to a computer and are controlled using a Python script, which allows to automatize the different measurements by controlling the parameters - magnetic field, dc current, rf power and sample support angle - and save the results.

Transport Measurements

The measurements presented in the results of this work are made at $\theta_H = 90°$, so that the applied magnetic field has only a perpendicular component. At this θ_H, we can study the magnetic configuration of the vortex and also of the SAF layer, which gain a perpendicular magnetization component as a fully perpendicular magnetic field, H_{perp}, is applied. These layers' magnetization increase in the direction of H_{perp}, and tend to become parallel for stronger fields, consequently reducing the average resistance of the device, R_0, as can be seen in Fig. 7. The R(H_{perp}) curve also shows the vortex core polarity switch, when there is a jump in resistance as the magnetic field is applied in the opposite direction of the vortex core magnetization.

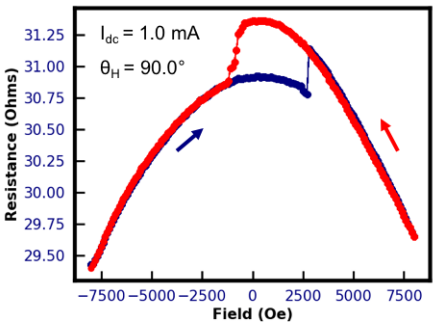

Figure 7: Evolution of the average resistance of the device with H_{perp}. The blue curve corresponds to the field sweep from -8.0 kOe to 8.0 kOe, while the red curve corresponds to the reverse sweep.

Spindiode Measurements

Four possible vortex configurations exist for the magnetic vortex: +C+P, +C-P, -C+P and -C-P. Both the chirality and polarity of the vortex core affect the studied phenomena, which means that before each measurement it is necessary to impose the vortex configuration. This is done through a preparation protocol:

1. a strong preparation current is injected into the device, imposing the vortex' chirality;
2. a perpendicular magnetic field, H_{perp}, strong enough to fix the vortex' polarity, is applied;
3. H_{perp} is decreased to zero;
4. the preparation current is also brought to zero.

During the experimental procedures of this work, the preparation was done with $H_{perp} = \pm 8.0$ kOe and $I_{dc} = \pm 8.0$ mA. Finally, after having imposed the vortex configuration we can perform what we call a spindiode measurement, which consists of measuring the voltage evolution at the device's terminals upon injection of an rf current, swept in a certain frequency range. This measurement can be made in different conditions, by varying the H_{perp}, the bias current, I_{dc}, and the power of the injected rf current, P_{rf}. A typical spindiode curve is shown in Fig. 8, where the rectification voltage due to the spin-torque diode effect appears at $f = 155$ MHz.

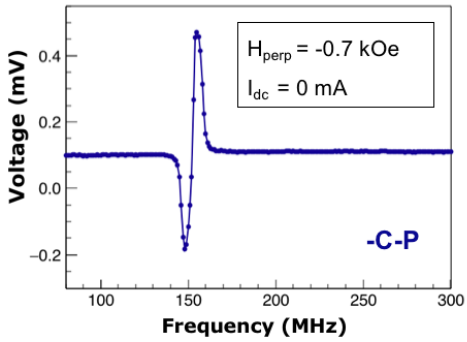

Figure 8: Example of spindiode measurement showing the rectified voltage due to the spin-torque diode effect at $f_{res} = 155$ MHz. Measurement performed for $H_{perp} = -0.7$ kOe, $I_{dc} = 0$ mA and $P_{rf} = -18$ mA, after vortex preparation in the -C-P configuration.

4. Vortex-based STOs for rf detection

The STO's operation can be divided into two different regimes: sub-critical and auto-oscillation regime. In the sub-critical regime, the dc current being injected into the STO does not provide a strong enough STT to overcome the damping term, meaning that there are no self-sustained oscillations of the vortex core. Furthermore, while there is no signal emission, the rf detection function can still be used, even without any bias current.

4.1. Spin-torque diode effect

In order to efficiently detect rf signals and, subsequently, harvest or transmit their power, it is important to understand and control certain properties of the spin-torque diode effect, such as the STO's resonance frequency, f_{res}, its maximum rectification voltage, ΔV, and its sensitivity, ϵ.

Perpendicular Magnetic Field

With the application of H_{perp}, the vortex' magnetization acquires a perpendicular component, $m_z = \frac{H_{perp}}{H_s}$, changing each of the applied forces acting on the vortex core, as described in 2.2. In Fig.9 (a), it is shown the evolution of f_{res} with H_{perp}, for an injected rf current power,$P_{rf} = -18$ dBm, prepared in the +C+P configuration, with no bias current applied. It is noticeable not only the linear increase in the resonance frequency, with the applied field's strength, but also an increase in ΔV. While the detection sensitivity is lower at zero H_{perp} than at stronger fields, it is relevant for future applications that STOs are capable of detecting/harvesting an rf signal without the need for a magnetic field being applied.

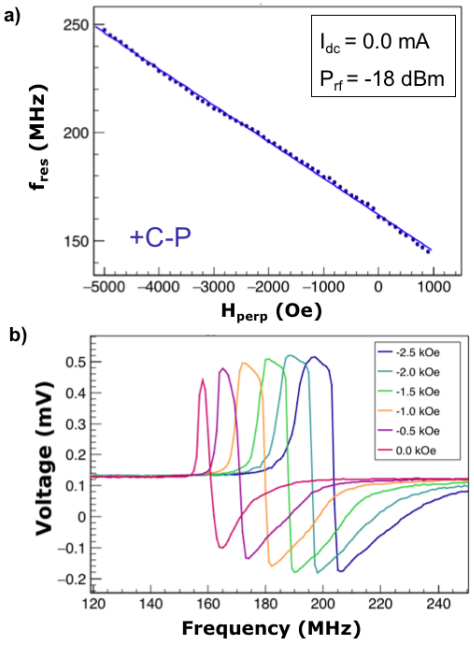

Figure 9: Experimental data from spindiode measurements at zero bias current and $P_{rf} = -18$ dBm ($I_{rf} = 0.02$ mA), in the +C-P configuration. a) STO's resonance frequency in function of the perpendicular magnetic field, H_{perp}. Data fit represented by the full line. b) Rectification voltage curves for different values of H_{perp}.

4.2. Bias Current

We measured the spindiode response of the STO in function of a small injected bias current between -0.8 mA and 0.8 mA, for the -C-P vortex configuration, $H_{perp} = -1.5$ kOe and $P_{rf} = -18$ dBm. The spin diode curves, taking into account only the voltage rectified due to the resistance variance, are presented in Fig. 10 a), together with the ΔV measured for each bias current, in Fig. 10 (b). Regarding the linewidth of the voltage response, we see that it increases for a positive bias current and it becomes smaller with the application of a negative current. On the other hand, f_{res} is not affected by the injection of a small bias current. As expected, the ΔV measured experimentally increases with a positive bias current, as the STT acts against the damping of the magnetization, and decreases for a negative current, due to the extra-damping effect. The variation in ΔV is more pronounced.

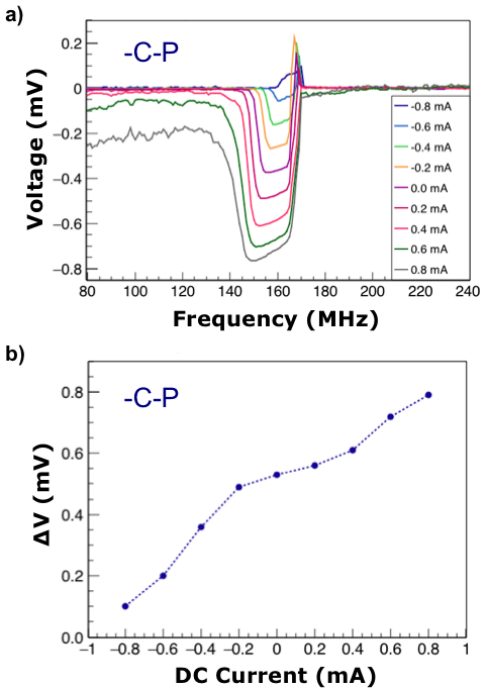

Figure 10: The rectification voltage increases with the bias current. a) Voltage response curves in function of the rf current's frequency. b) Measured ΔV as a function of I_{dc}. Measurements performed for $H_{perp} = -1.5$ kOe and $P_{rf} = -18$ dBm.

4.3. Influence of the vortex chirality and polarity on the rectification response

As mentioned before, the vortex has four possible configurations, set before each measurement, which affect its behavior, notably the spin-torque diode effect. We measured the spin-torque diode response, at $I_{dc} = 0.0$ mA, in a range from -6.0 kOe to 6.0 kOe, for the different vortex configurations. We determined that, to change the polarity of the vortex core, in the studied oscillator, a magnetic field stronger than ± 2.5 kOe is needed. Furthermore, there is a bistability of the polarity between -0.9 kOe and 0.9 kOe. In the bistable region, the rectification response depends simply on the direction of the magnetic field in the preparation protocol. The linear behavior of the resonance frequency, described in the previous section is valid for the different configurations, although there is a shift in the resonance frequencies for different chiralities, likely due to the presence of non-compensated stray fields in the SAF layer. For example, in the -C-P configuration $f_{res}(0) = 140$ MHz, while in the opposite chirality, +C-P, $f_{res}(0) = 160$ MHz.

5. Serial connection of vortex STOs: towards higher detection sensitivity

In order to use STOs in efficient energy harvesting and transmission applications, we must strive to improve the sensitivity of our detection system. With higher sensitivities, we'll be able to detect lower power signals and improve the rf to dc conversion. An approach to this is to connect several STOs in series, with very close eigenfrequencies, so that they have a simultaneous rectification response when an rf signal at such frequencies is injected into the circuit. In a simple approximation, we could expect a simple sum of the rectification voltage of each oscillator.

5.1. Rectification response for two STOs in series

The STOs studied in this chapter have very close resonance frequencies, which means the vortices' resonant modes are excited and both STOs exhibit the spindiode effect simultaneously. As such, we expect a rectification voltage in the range of the STOs eigenfrequencies with a shape similar to the sum of each STO's response.

Comparison with single STO case

The experimental results, presented in Fig. 11, correspond to the -C+P configuration of the vortex in each STO, without any applied dc current and magnetic field. In the figure, we present the spindiode power map, for P_{rf} between -20.0 dBm and -12.0 dBm, and the spindiode curve at $P_{rf} = -14$ dBm, for each STO on their own, as well as for their serial connection. By comparing the power maps obtained for STO A (Fig. 11(a)) and STO B (Fig. 11(b)), we see that the linewidth of the rectification effect is larger for STO B than for STO A, for higher injection powers. STO A exhibits a measurable rectification voltage down to -20 dBm between 140 MHz and 160 MHz, in the measured P_{rf} range. On the other hand, the spindiode rectification effect in STO B, is

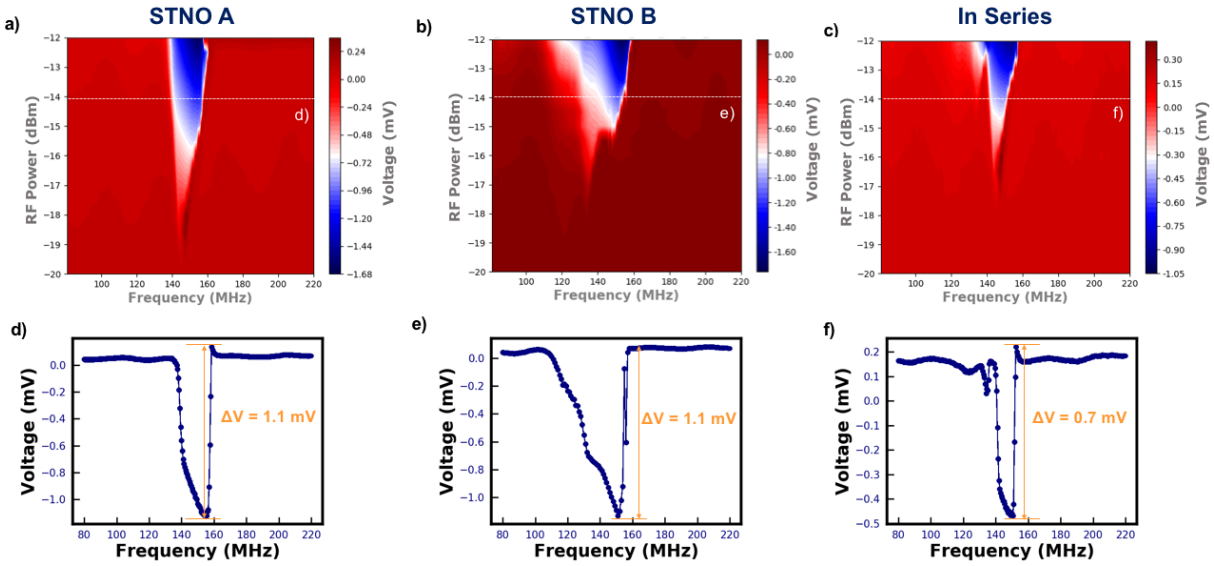

Figure 11: a,b,c) Voltage rectification response with the injected rf current's frequency and power, for STO A, STO B and the case where STO A and STO B are connected in series. d,e,f) Respective voltage response for the specific case $P_{rf} = -14$ dBm. These results were obtained for the -C+P vortex configuration, at $H_{perp} = 0$ kOe and $I_{dc} = 0$ mA.

measurable only down to $P_{rf} = -18$ dBm and, below -15 dBm, the maximum ΔV shifts to lower frequencies (130-140 MHz).

The measured rectification voltage in the case where two STOs are connected in series (Fig. 11(e,f)) is actually smaller than that of the each STO on its own, and reaches around a third of the expected value, for the same P_{rf}. For $P_{rf} = -14$ dBm, each STO on its own has $\Delta V_A = \Delta V_B = 1.1$ mV, as seen in Fig. 11(b,d),while, in the case where they are connected in series, the response is of 0.7 mV (Fig. 11(f)), much lower than the expected value $\Delta V_{expected} \approx 2.2$ mV.

The observed decrease in detection sensitivity for two STOs in series may be due to different factors. We propose that the most relevant is the increase in the impedance mismatch of the system due to the connection of the second STO. The maximum power-transfer theorem states that maximum power is transferred from the rf source to the load (STOs A and B) when the load impedance, $Z_{Series} = Z_A + Z_B$, equals the source's impedance $Z_0 = 50\Omega$.

As previously stated, the objective of connecting two STOs in series is to improve the system's sensitivity: have a higher rectification voltage, for a lower input power. In order to achieve this goal we need to understand, firstly, why the expected results are not obtained by considering the different factors mentioned above.

Power loss in serial connection of STOs

We compare the experimental spindiode results obtained for the connection in series , at $P_{rf} = -14.0, -12.5, -11.0$ dBm, $H_{perp} = 0$ and $I_{dc} = 0$, with the expected voltage curve for $P_{rf} = -14.0$ dBm, given by the sum of the results obtained for each STO in the same measurement conditions, in Fig. 12(a). Comparing the experimental and expected results, shown respectively in yellow and blue in Fig. 12(b), it is apparent the difference between ΔV_{Series} and $\Delta V_{Expected}$ described above. On the other hand, for an rf input of -11.0 dBm, the resulting spindiode curve resembles very closely the expected -14.0 dBm curve. This suggests that the rf power being transferred to the oscillators, when connected in series, is at least 3 dBm lower than in the case where they are measured each on their own. A 3 dBm decrease of the effective rf power corresponds to halving the power available to the STOs.

ΔV_{Series} was measured for P_{rf} between -17.0 dBm and -10.0 dBm and the measurements are presented in yellow in Fig. 12(b), while the blue curve represents $\Delta V_{Expected}$. There is a "shift" between the two mentioned curves, as seen before in the case $P_{rf} = -14.0$ dBm, which corresponds to the power loss, P_{lost} due to connecting the oscillators in series.

We measure the system's power losses using a 2-port Vector Network Analyzer (VNA), which is an instrument that allows to test rf components by injecting a known stimulus signal into it and then measuring the reflected and transmitted signals. The transmitted and reflected amplitudes of a -15 dBm signal are measured, for a frequency range of 100-300 MHz. The measurements were

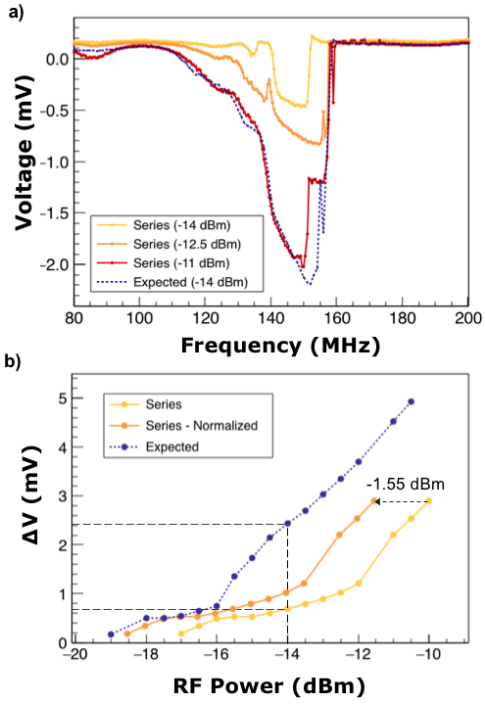

Figure 12: Spin-torque diode measurements for the -C+P vortex configuration, at $H_{perp} = 0$ kOe and $I_{dc} = 0$ mA. a) Variation of the voltage response for $P_{rf} = -14.0, -12.5, -11.0$ dBm, for the serial connection configuration, and expected response for $P_{rf} = -14.0$ dBm. b) Evolution of ΔV voltage with P_{rf}.

performed for STO A, STO B and the case that both are connected in series, Fig. 13(a). In this figure, both the transmission (S_{12}) and reflection (S_{11}) parameters are shown: the top 3 curves corresponding to the former, while the bottom curves correspond to the latter. During the measurement, no external magnetic field or dc current are being applied to the system in study.

We consider the S-parameters in the frequency range between 140-160 MHz, englobing STOs' A and B resonance frequencies. The average power losses, measured by the S_{12} parameter, and the power ratios, given by $\frac{P_2}{P_1} = 10^{S_{12}/10}$, are shown in Table 2. The rf power losses when a single oscillator is connected have a large impact in the system's sensitivity, with only about a third of the signal being transmitted.

While in the previous section, we estimated that the relative power losses between the single and double STO cases was around 0.5 (−3 dB), the VNA measurements show a relative power ratio of 0.70 due to impedance mismatch. By normalizing the spindiode experimental results to already take into account the −1.55 dB measured loss (orange curve in Fig. 12), we can see that it approaches the expected ΔV (blue curve). There is still a fraction of the power losses between the two instances

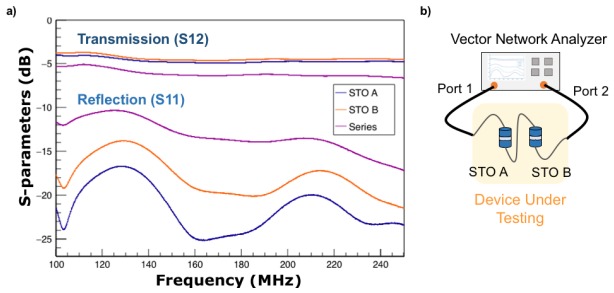

Figure 13: a) Transmission (S_{12}) and Reflection (S_{11}) parameters with the injected signal's frequency, for STO A, STO B and the case where both are connected in series. Measurements made with an injected signal power of −15 dBm. b) VNA measurement setup.

which is not accounted for in the measurements performed.

While the measured power losses between the single STO and double STO cases are not negligible (−1.55 dB), there are even more significant losses in the single STO case to begin with, reaching over −4.5 dB. Only a fraction of the injected power is effectively exciting the vortices' magnetization and giving rise to the spin-torque diode effect. If we're able to decrease these losses there will be a great increase in the sensitivity of the systems in study. In order to do so it is necessary to improve its impedance matching by adapting the device's impedance to Z_0. Ideally, STOs are purely resistive devices, but in practice they have a reactive component which makes impedance matching more complex.

5.2. Direct current in STO's antenna

We study the effect of a dc current passing through the STO's antenna in the rectification response of two oscillators connected in series. These experimental results were obtained for a different set of oscillators than those used in the previous sections, although with similar characteristics, referred to as STOs C and D. The STOs were connected in series as previously, with the addition of having a second dc current source connected to one of the oscillators' antenna (STO D).

We measure the rectification response of the oscillators to an rf current, with $P_{rf} = -14$ dBm, for $H_{perp} = -0.8$ kOe and $I_{dc} = -0.8$ mA. For $I_{antD} = 0$ (Fig. 14(a)), $\Delta V_{Series} = 0.95$ mV, and its not possible to distinguish the response from each oscillator. By applying a dc current through the antenna, I_{antD}, an in-plane magnetic field is created at the STO's free layer, affecting its magnetization and consequently its resonance frequency. For $I_{antD} = 18$ mA (Fig. 14(b)), f_{res} of STO D shifts to higher values, making it possible to distinguish clearly both rectification voltage peaks. The

Table 2: Average power loss (S_{12}) and power ratio in the 140-160 MHz frequency range. The power loss error is given by the sample's standard deviation.

	STNO A	STNO B	In Series	Relative Loss
Power Loss (dB)	-4.82 ± 0.04	-4.57 ± 0.03	-6.25 ± 0.06	-1.55 ± 0.09
Power ratio	0.33 ± 0.01	0.35 ± 0.01	0.24 ± 0.01	0.70 ± 0.02

first peak corresponds to the voltage rectified by STO C, which is independent of the current applied to the other STO's antenna, while the second peak corresponds to STO D.

The sum of both peaks' ΔV is of 0.98 mV, which is very close to $\Delta V_{Series} = 0.95$, measured at $I_{antD} = 0$ mV. Assuming that I_{ant} has no influence in the voltage amplitude, these measurements confirm the hypothesis that the total rectification voltage in the case where the oscillators are connected in series is simply the sum of each oscillators' response.

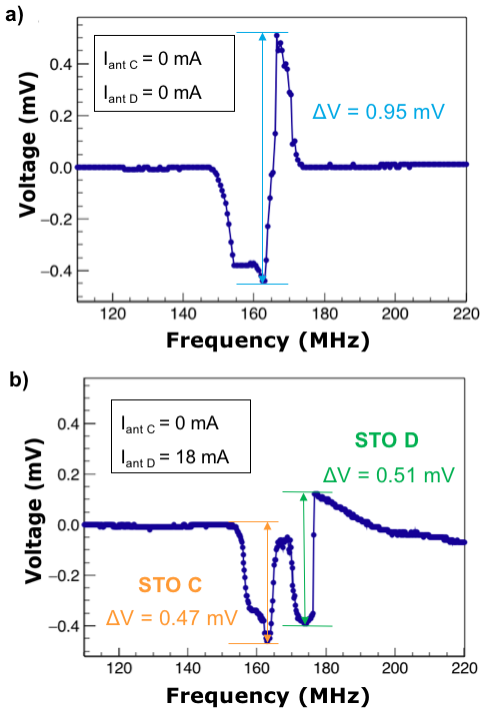

Figure 14: Evolution of the voltage response due to the spin-torque diode effect, at $H_{perp} = -0.8$ kOe, $I_{dc} = -0.8$ mA and $P_{rf} = -14$ dBm. a) Without any dc current injected into the antennae. b) With an 18 mA current in STO's D antenna, I_{antD}.

We've shown that for an equal circuit, and equal impedance matching, the system's sensitivity is roughly doubled by having two STOs with the same resonance frequency connected in series. We can expect that, when connecting N similar STOs, we can linearly scale the rf to dc conversion by N.

6. Conclusions

The objective for this work was to make way to the increase of the rf-to-dc conversion in single vortex based STOs, in order to approach an efficient application of these devices in rf detection and energy harvesting technologies. As shown, the spin-torque diode rectification effect can operate at zero external magnetic field and zero bias current, which is an advantage in terms of energy consumption in future device integration, although a magnetic field and the injection of a dc current is still needed to impose the vortex' polarity and chirality, respectively.

During this project we focused on increasing the system's sensitivity through the connection of more than one STO, comparing between the single STO case and the double STO case, in the same measurement conditions. We connected two similar oscillators in series, expecting the sensitivity of this system, for a given injection power, to be $\epsilon_{Series} = \epsilon_{STOA} + \epsilon_{STOB}$. It was found that when two oscillators are connected in series, the impedance matching of the system declines, which translates in a loss of the power being injected into the device, diminishing the system's sensitivity compared to the case where only a single oscillator is connected. The comparison between the expected rectification voltage for a certain P_{rf} and the experimentally measured results, suggested that around half (-3 dB) of the injected power was lost from one case to the other. In the measurements done with a VNA, it was found that the relative power loss between those two cases was actually smaller than previously suggested, with $(30 \pm 2)\%$ less power being transmitted when two oscillators are connected in series. On top of this, the Vector Network Analyzer results showed that the absolute losses are very large, even when only one oscillator is connected, with about 2/3 of the source's power being lost.

While the results obtained in this work don't yet show an increase in the detection sensitivity, by scaling the system to two STOs, it was shown in this work that it is possible to do so and, most importantly, which are the obstacles to tackle ahead. In future works, a more in depth study of the rf characteristics of STOs on their own must be done,

in order to design solutions to adapt the circuit's impedance. If this is done successfully for a two-STO system, it will then be possible to systematically scale it to larger and larger STO networks. Furthermore, this type of system can be greatly improved in the future through the nano-fabrication process, such as reducing the variability between the STOs in a chip, or designing STOs with higher TMRs, in order to improve their sensitivity.

At last, in a broader perspective, this work is part of the first effort to scale the use of STOs as energy harvesters. Designing ultra sensitive rf energy harvesters by using STO networks can have a huge impact in the ICT area, with the increase of IoT devices, which need to be wireless, with low power consumption and compact.

References

[1] Ebels, U., Hem, J., Purbawati, A., Calafora, A. R., Murapaka, C., Vila, L., Merazzo, K. J., Jimenez, E., Cyrille, M.-C., Ferreira, R., Kreissig, M., Ma, R., Ellinger, F., Lebrun, R., Wittrock, S., Cros, V., and Bortolotti, P. In *2017 Joint Conference of the European Frequency and Time Forum and IEEE International Frequency Control Symposium (EFTF/IFC)*, 66–67. IEEE, jul (2017).

[2] Locatelli, N., Cros, V., and Grollier, J. *Nature Materials* **13**(1), 11–20 jan (2014).

[3] Khvalkovskiy, A. V., Grollier, J., Dussaux, A., Zvezdin, K. A., and Cros, V. *Physical Review B - Condensed Matter and Materials Physics* (2009).

[4] Dussaux, A., Khvalkovskiy, A. V., Bortolotti, P., Grollier, J., Cros, V., and Fert, A. *Physical Review B* **86**(1), 014402 jul (2012).

[5] Lebrun, R. *Coupled vortex dynamics in spin-torque oscillators: From resonant excitation to mutual synchronization.* PhD thesis, Université Paris-Saclay, (2015).

[6] Tulapurkar, A. A., Suzuki, Y., Fukushima, A., Kubota, H., Maehara, H., Tsunekawa, K., Djayaprawira, D. D., Watanabe, N., and Yuasa, S. *Nature* **438**(7066), 339–342 nov (2005).

[7] Miwa, S., Ishibashi, S., Tomita, H., Nozaki, T., Tamura, E., Ando, K., Mizuochi, N., Saruya, T., Kubota, H., Yakushiji, K., Taniguchi, T., Imamura, H., Fukushima, A., Yuasa, S., and Suzuki, Y. *Nature Materials* **13**(1), 50–56 jan (2014).

[8] Zhang, L., Fang, B., Cai, J., Carpentieri, M., Puliafito, V., Garescì, F., Amiri, P. K., Finocchio, G., and Zeng, Z. *Applied Physics Letters* (2018).

[9] Jenkins, A. S., Lebrun, R., Grimaldi, E., Tsunegi, S., Bortolotti, P., Kubota, H., Yakushiji, K., Fukushima, A., de Loubens, G., Klein, O., Yuasa, S., and Cros, V. *Nature Nanotechnology* **11**(4), 360–364 jan (2016).

[10] Tsunegi, S., Taniguchi, T., Lebrun, R., Yakushiji, K., Cros, V., Grollier, J., Fukushima, A., Yuasa, S., and Kubota, H. *Scientific Reports* **8**(1), 13475 dec (2018).